A surface modified ODS superalloy by thermal oxidation for potential implant applications

M. C. GARCÍA-ALONSO[1], J. L. GONZÁLEZ-CARRASCO[1,*], P. PÉREZ[2], V. A. C. HAANAPPEL[2], M. L. ESCUDERO[1], J. CHAO[1], M. F. STROOSNIJDER[2]
[1]*Centro Nacional de Investigaciones Metalúrgicas, CENIM-CSIC, Avda. Gregorio del Amo 8, 28040 Madrid, Spain*
[2]*Joint Research Center of the European Commission, Institute for Health and Consumer Protection, 21020 Ispra (VA), Italy*
E-mail: jlg@cenim.csic.es

In the present work attention is paid on the composition, structure and protective properties of alumina layer produced by high temperature oxidation on MA 956 superalloy (Fe-20Cr-4.5Al-0.5Ti-0.5Y_2O_3 (wt%)). The combination of good mechanical properties of this material and the excellent biocompatibility, the good wear and corrosion behavior of an outer α-alumina layer, limiting the release of ionic species and wear debris from the bulk material into the body-fluid environment, can make this material a candidate alloy for medical applications. Isothermal oxidation at 1100 °C in air of the alloy has led to the formation of a fine-grained, compact and adherent α-alumina scale. Oxide nodules rich in Ti, Y, Cr, and Fe were found on the top of the surface. *In vitro* electrochemical corrosion experiments showed good protective properties of the oxide scale. Moreover, no spallation of the alumina layer was observed. This feature is significant considering that the alumina layer has to withstand very high compressive stresses resulting from both growth and thermal stresses incorporated during cooling.

1. Introduction

Metals and alloys are the most common materials used as surgical implants for load-bearing joint replacements (e.g. hip or knee) because of their mechanical stability and acceptable corrosion resistance. Since the early 1960s, at which the first Charnley prosthesis was made, the most long-standing combination nowadays is the couple between an ultra high molecular weight polyethylene (UHMWPE) and a ball of CoCr alloy, performing well for a period between 10 and 15 years. This system did not provoke relatively trouble considering that life expectancy of the older patients was not too long. The increased life expectancy and the necessity of implanting devices in younger patients, are the driving forces for the development of materials that will be able to perform well for a longer period.

There is now sufficient evidence that the major cause for failure of total hip or knee arthroplasties is osteolysis, which is associated with the gradual accumulation of wear debris in the periprosthetic tissue [1]. Modification of the bulk properties, the surface of the alloy, e.g. by means of dispersion hardening or implantation of nitrogen or other atoms, and the subsurface of the UHMWPE, e.g. by cross-linking, are some possibilities to increase the wear resistance [2]. Another improvement might be the replacement of the metal by a ceramic femoral head, which is reported to produce less polyethylene wear than metal-UHMWPE couples [3]. Monolithic ceramics, however, are inherently brittle and fabrication is constricted, specially when considering recent improvements of the prosthesis design.

The development of alumina coated alloys has also received considerable attention because the resulting material could combine the inherent mechanical properties of the substrate, with the superior biocompatibility of the outer alumina layer. Despite this potential, however, the use of alumina layers processed by plasma spraying, PVD and CVD techniques [4–6] are not yet commonly applied to metallic biomaterials since biochemical and mechanical properties of the coatings substantially depends on the presence of defects, and the type and microstructure of the formed alumina [4]. For example, metastable alumina, such as θ- and δ-alumina has a lower density and a much lower hardness than α-alumina. Moreover, these compounds are soluble in a variety of acids, a property that should be taken into consideration because of acidification of the environment in case of infections. Hence the development of hard, thermally and chemically stable α-Al_2O_3 layers is a preferred objective of process development.

In this respect, thermal oxidation treatments have emerged as a technique easier to perform and more

*Author to whom correspondence should be addressed.

efficient than other ceramic coating processes such as plasma spraying, PVD and CVD techniques [5–7]. In the research field of biomaterials, thermal oxidation has already been successfully used to produce *in situ* zirconia [8–15] and alumina [16–19] ''coated'' materials. The former coating has been formed on Ti-Nb-Zr or Zr-Nb base alloys and the second on MA 956, a ferritic superalloy widely used for high temperature applications.

The present work aims to an in-depth characterisation of the alumina layer generated at high temperature on MA 956 superalloy. The nature, composition and protective properties of the alumina layer in turn will determine the interaction with the biological environment. Protective properties of the scale in physiological media are evaluated using electrochemical impedance spectroscopy (EIS).

2. Materials and methods

INCOLOY ODS MA 956 with a nominal composition of Fe-20Cr-4.5Al-0.5Ti-0.5Y_2O_3 (wt %) is an oxide dispersion strengthened (ODS) alloy obtained by a powder metallurgy route consisting of mechanical alloying (MA) and a thermo-mechanical treatment at elevated temperatures. The material used in this research was supplied by Inco Alloys International (Hereford, UK) as hot rolled bars of 9.5 mm in diameter. Annealing of the bar at 1100 °C (or above) caused a grain growth and a change from the $\langle 110 \rangle$ to the $\langle 100 \rangle$ texture, which corresponds with the lowest Young's modulus (about 150 GPa) [20–22]. It is worth to mention that the texture of the material was not changed during the thermal oxidation treatment used in this study.

Specimens used for different experiments were removed from the core of the bar. Before testing, all major surfaces were abraded on successively finer silicon carbide papers, and finally mechanically polished with 1 μm diamond paste to achieve a mirror-like surface finish. Prior to oxidation, all specimens were ultrasonically cleaned with alcohol.

Alumina layers with various thicknesses were obtained by thermal oxidation at 1100 °C in air for 1, 3 and 100 h. This temperature was selected on the basis of a preliminary study [23] focusing on the oxidation and corrosion behavior. To determine the oxidation kinetics, specimens were periodically taken out of the furnace and weighed by using a microbalance with an accuracy of 10 μg.

Characterization of the microstructure has been performed using optical metallography, scanning electron microscopy (SEM), energy dispersive X-ray microanalysis (EDX) and glancing angle X-ray diffraction (GAXRD). The spectra were analyzed using JCPDS standards.

Roughness measurements calculating the average roughness R_a over a surface area of $3.0 \times 3.0\,mm^2$ were performed before and after the oxidation treatments using a Rodenstock RM600 laser profilometer.

Element distribution through the scale was investigated by means of a radio frequency glow discharge optical emission source (GDOES), using a Jobin Yvon JY5000RF instrument. The settings (discharge gas pressure approximately 10 mbar, RF power = 40 W) were adjusted for optimum depth resolution.

Electrochemical impedance spectroscopic measurements (EIS) were carried out using a 1250 Solartron frequency analyzer and a 273 EG & G potentiostat. The experiments were conducted at room temperature in Hank's solution (Table I) for both non-treated and treated specimens, simulating the aggressive environment of bodily fluids. Measurements were performed applying a sinusoidal potential of 10 mV in amplitude to the working electrode. The frequencies varied from 64 kHz to 1 mHz. A saturated calomel and platinum electrodes were used as reference and counter electrodes, respectively.

3. Results

3.1. Scale growth kinetics

Fig. 1 shows the mass change of MA 956 *vs.* exposure time at 1100 °C. To analyze the growth kinetics, the mass gain curve is fitted to a power type law of the form:

$$(\Delta W) = kt^n$$

where ΔW is the mass gain per unit area, k is the oxidation rate constant, n is the exponential factor, and t is the exposure time. For shorter exposure times (< 50 h) the kinetics can be described by a parabolic type law ($n \approx 0.5$) indicating that the oxidation process is diffusion controled. For longer exposure times a slightly lower value of n was obtained, representative for subparabolic type behavior. A deeper analysis of the oxidation kinetics of this alloy has been recently revised elsewhere [23, 24].

3.2. Structure and composition of the oxide scale

Characterization of the surface morphology of alumina layers formed at 1, 3 and 100 h at 1100 °C has been performed. As an example, Fig. 2a and b show SEM micrographs of the oxidized specimen surfaces after 3

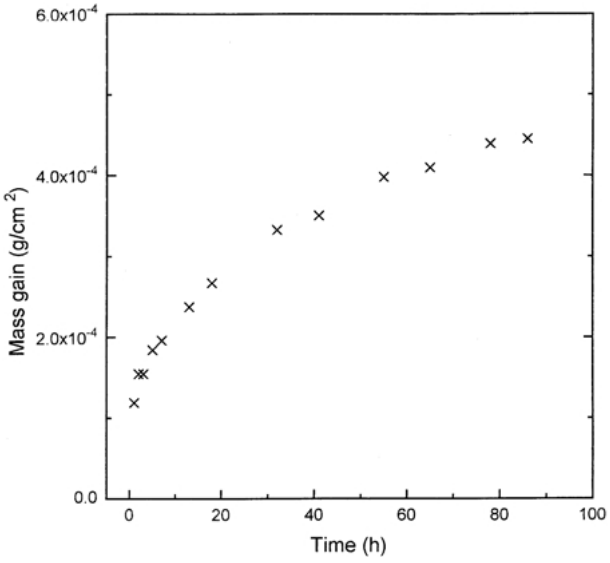

Figure 1 Mass change per unit area of MA 956 as a function of the exposure time at 1100 °C.

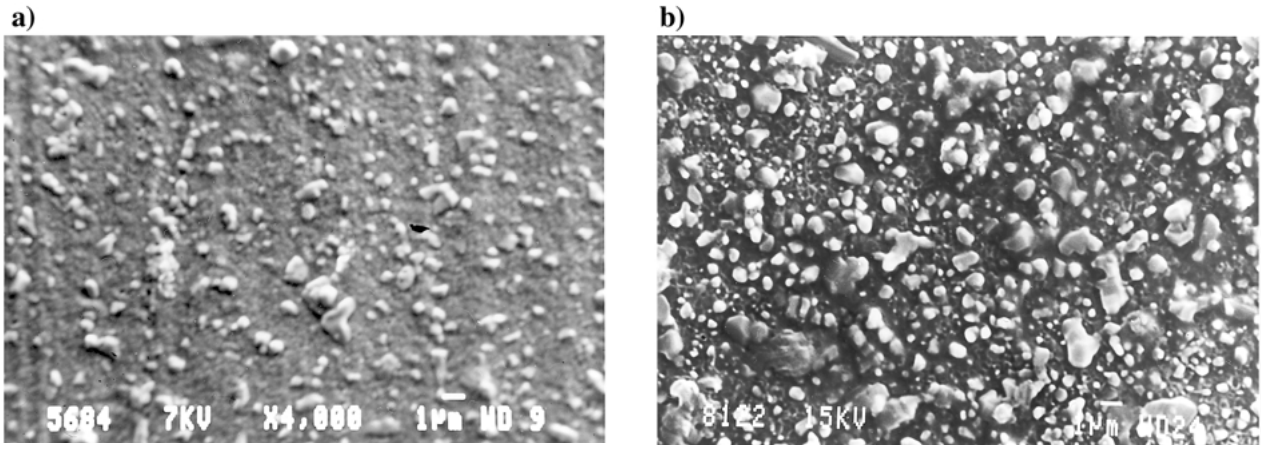

Figure 2 SEM micrograph of the surface morphology of MA 956 after oxidation in air at 1100 °C for: (a) 3 h and (b) 100 h exposure.

TABLE I Chemical composition of Hank's solution

Composition	Concentration g/l
NaCl	8.00
$CaCl_2$	0.14
KCl	0.40
$NaCO_3H$	0.35
Glucosa	1.00
$MgCl_2 \cdot 6H_2O$	0.10
$Na_2PO_4H \cdot 2H_2O$	0.06
KPO_4H_2	0.06
$MgSO_4 \cdot 7H_2O$	0.06

and 100 h at 1100 °C. An homogeneous scale without any indication of scale spallation is formed. Only a narrow zone at the specimen edge showed some spallation after cooling due to significant stresses, which is induced by the small edge radius. The scale surface reveals the presence of small nodules growing on the outer part of a nearly pure alumina scale. The total number and size of these nodules slightly increased with increasing exposure time. For short exposure times (Fig. 2a) these nodules were seldom larger than 1 μm. After 100 h exposure, although some nodules grew to about 3 μm in diameter, the major part was smaller than 1 μm (Fig. 2b).

Surface roughness measurements performed before and after oxidation revealed an increase of the average roughness R_a from 0.080 μm in the initial polished condition, to 0.50 and 0.65 μm after 3 and 100 h exposure, respectively, probably associated to the formation of nodules.

The structure of the scales has been studied by GAXRD. Fig. 3(a–d) show the diffraction spectra at 1° angle of incidence of the oxide scale formed after 1, 3 and 100 h exposure and comparatively, of the non-oxidized material, respectively. For the experimental conditions used for GAXRD the penetration depth is 1.4 μm for pure α-Al_2O_3. After 1 h oxidation (Fig. 3(a)) a thin scale was formed, mainly consisting of α-Al_2O_3. Together to the α-Al_2O_3 phase, small peaks from Fe and Cr mixed oxide compounds (probably $FeCr_2O_4$, spinel) are present but in a minor extent. Similar observations were found for the oxide scale formed upon 3 h (Fig. 3(b)). In addition, small peaks probably corresponding to Ti and Y mixed oxides (Y_2TiO_5) started to appear.

After 100 h exposure (Fig. 3(c)) more phases were identified. In this case, next to the high contribution of peaks from the α-Al_2O_3 also peaks from TiO_2 (rutile) and probably (Y_2TiO_5) were identified. To get more information from the outer surface layer, GAXRD analyzes were repeated with 0.5° angle of incidence (penetration depth in α-Al_2O_3: 0.7 μm) for oxidized samples treated after 100 h of exposure. The relative intensities of the previously mentioned peaks, compared to those from α-Al_2O_3, are increased, indicating that these compounds are more pronounced at the outer part of the oxide scale. Additionally, no peaks from the underlying substrate were found anymore, due to thickening of the oxide scale.

3.3. Cross-sectional analyses

Cross sectional observations of the oxidized samples revealed the formation of a smooth oxide scale, irrespective the exposure time. After 1, 3 and 100 h

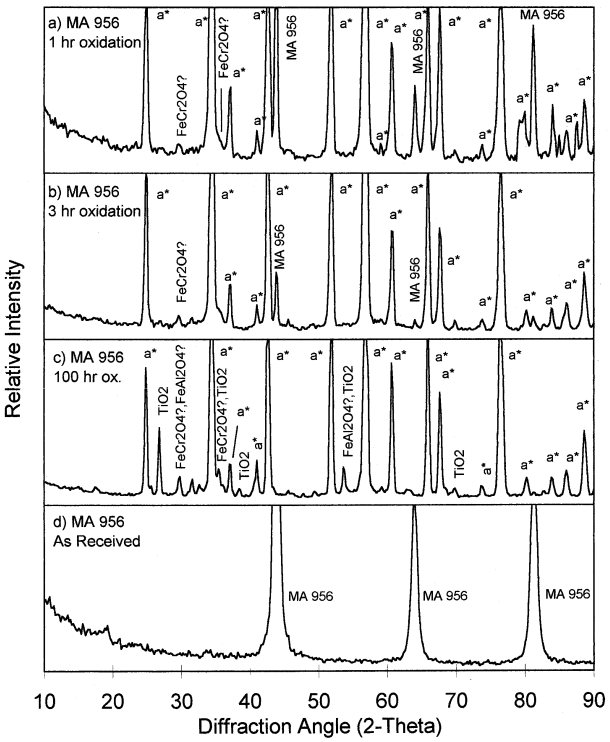

Figure 3 GAXRD diffraction spectra at 1° angle of incidence of the oxide scales formed on MA 956 after 1, 3 and 100 h exposure including the GAXRD pattern of a non-oxidized MA 956 specimen (the intensity scale is magnified 10 times); a = α-Al_2O_3.

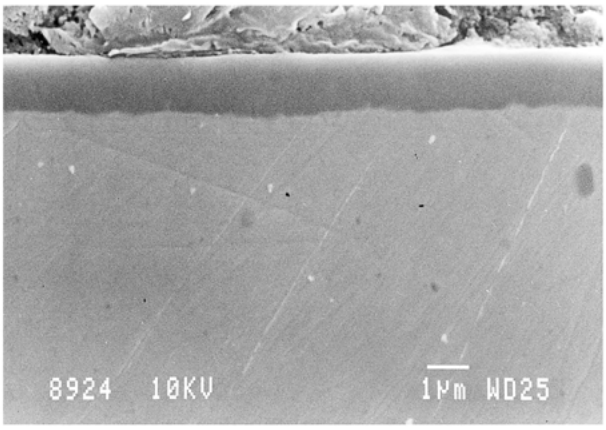

Figure 4 Cross sectional view of MA 956 oxidized at 1100 °C for 100 h exposure.

exposure the thickness of the oxide scale was about 0.7, 1 and 4 µm, respectively. Fig. 4 shows the cross-section micrograph for the 100 h-oxidized specimen. Neither cracking nor void formation at the scale/metal interface was observed on all of the specimens indicative of a good adherence of the oxide scale, apart from scale detachment observed at the specimen edges. Examination by SEM of the fractured scale at these regions revealed small equiaxed grains on top of larger columnar grains (Fig. 5). This scale microstructure is the typical for yttria-doped alumina scales and denotes the grain size increase of the alumina in the scale-growth direction, i.e. from the free surface to the scale-metal interphase.

Analysis of the in-depth element distribution of the scale was performed by GDOES. Fig. 6(a) and (b) shows the elemental profiles versus sputter time of MA 956 oxidized for 3 and 100 h, respectively. The emission intensities were normalized with respect to the argon emission intensity. From these results it is clear that a high amount of Aluminum and oxygen were found at the outer part of the scale, indicative of the formation of alumina. For sake of clarity it should be stated that variation of elements in the vicinity of the outer surface is quite small and its existence only becomes clearly apparent in the logarithmic plot. Additionally, at the outer part of the scale surface enrichment of Y and Ti is observed. Just below the outer surface of the scale some enrichment of Fe and Cr occurred. Similar observations

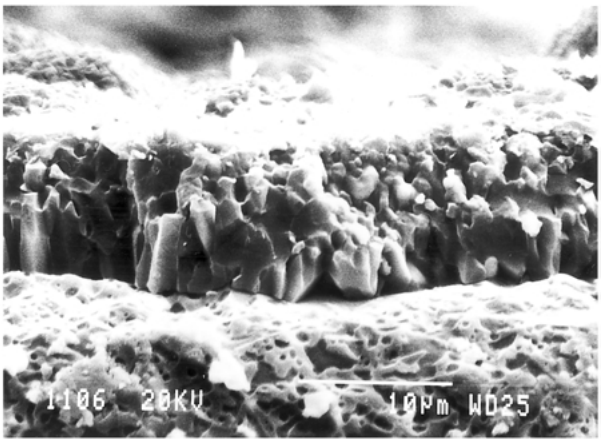

Figure 5 SEM micrograph of oxidized MA 956 after 100 h at 1100 °C with some spallation of the formed oxide scale near the edge of the sample.

were found after 100 h exposure. The relative peak intensities corresponding with Ti and Y at the outer surface increased with increasing oxidation time.

3.4. Protective properties

The protective properties of the scale were evaluated by electrochemical impedance spectroscopy. Figs 7 and 8 show the Nyquist and Bode diagrams, respectively, for the as-received and pre-oxidized specimens (1, 3 and 100 h) after four days of immersion in Hank's solution. The Nyquist plot (Fig. 7) shows a very wide arc with elevated impedance values, indicating a high corrosion resistance. For the as-received condition, the good corrosion behavior is provided by the passive film, and for preoxidized specimens by the alumina layer formed already upon 1 h oxidation. The impedance values obtained by preoxidized samples are four orders of magnitude higher than for the as-received specimens, which shows the superior corrosion behavior for preoxidized samples. This fact is more evident in the Bode diagram (Fig. 8), where the modulus of the impedance vector Z is given as function of the frequency f. The absence of a low-frequency plateau means that the resistance of the alumina layer is significantly high ($> 10^{10}\,\Omega\,\mathrm{cm}^2$). This high value shows the high protection of the alumina layer. This observation is also supported by the phase angle Bode plot, where a phase angle close to $-90°$ has been measured for the whole range of frequencies, typically for a capacitive behavior of the oxide layer.

4. Discussion

A wide range of metallic alloys have already been used for surgical implant devices, each one with its own advantages and drawbacks. The most ideal bio-material being used for load-bearing joint replacements should exhibit at least the following optimum properties: (1) a Young's modulus corresponding more or less with the modulus of the bone (10–40 GPa), (2) a high friction and wear resistance in order to suppress the formation of third body particles, (3) an excellent biocompatibility indicated by the absence of adverse tissue reactions, (4) an excellent corrosion resistance against bodily fluids, and (5) an acceptable strength to withstand cycling loading.

Young's modulus, yield strength, and ultimate strength of conventional and potential bio-materials are shown in Table II. From this table it is clear than common biomaterials (Co-Cr-Mo, SS 316L, Ti-6Al-4V, Ti-6Al-7Nb) have elastic moduli which significantly differ from that of the bone. A too large difference between the moduli of the bone and the bio-material limits the ability to transfer load to the surrounding bone environment, which eventually may result in prosthesis failure. To optimize the Young's modulus of orthopaedic devices, several titanium-containing alloys having a Young's modulus rather close to that of the bone have been developed. However, developing a material with a low Young's modulus does not automatically improve the other properties, such as optimization of the tribological properties. Especially titanium-containing alloys do not always exhibit a satisfactory friction and wear behavior

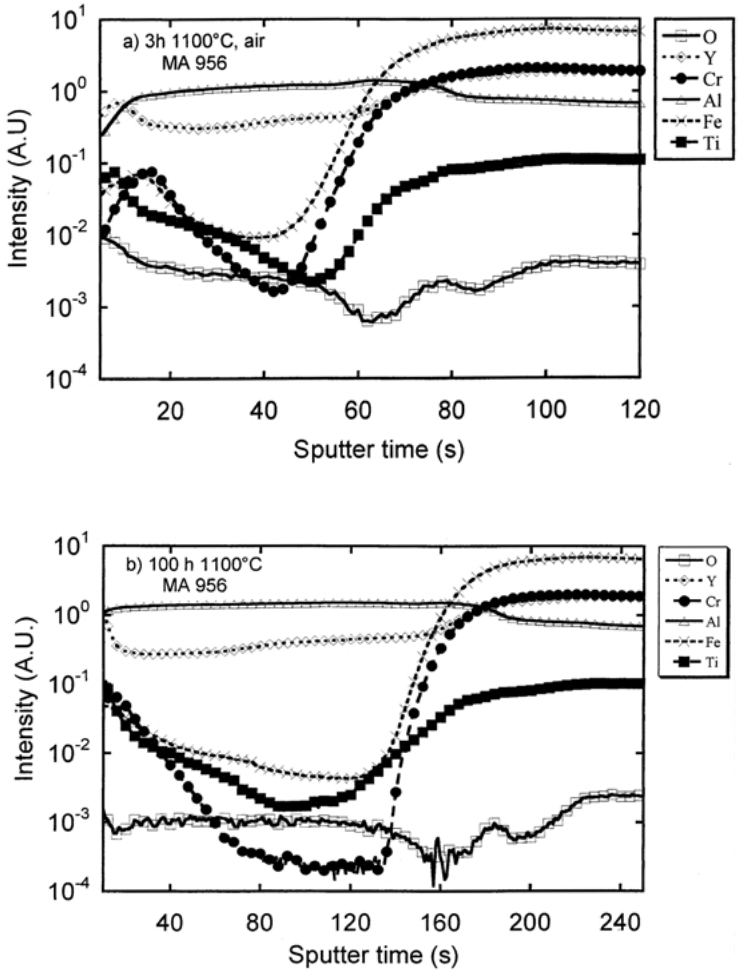

Figure 6 Intensity versus sputter time of the oxide scale developed on MA 956 at 1100 °C after: (a) 3 h, and (b) 100 h exposure.

[26]. To overcome these difficulties, a large amount of effort has been devoted [see e.g. Lemons [27], and references therein] to study the effect of surface modification each with their own characteristics, such as ion implantation, plasma spraying, chemical and physical vapor deposition, anodisation, nitriding, etc. of existing metallic biomaterials. These techniques have been used as a means to improve their surface properties on the long-term performance of orthopaedic implants without affecting detrimentally their required mechanical properties and their biocompatibility.

The development of ceramic coated bio-materials by techniques such as plasma spraying, CVD, and PVD has received considerable attention because the modified alloy could combine the inherent mechanical properties of the substrate with the good properties of an outer ceramic layer [28]. However, the resulting coating is relatively thick and may contain micro-cracks or pores, which would favor cracking or peeling off of the coating during service. Moreover, the residual stresses in the coatings are slightly compressive or even tensile, which could impair fatigue and wear behavior. In this respect, a thermal oxidation of the base alloy might overcome the problems related to overlay coatings. Generally, this treatment induces highly compressive residual stresses in the scale. This may represent a great advantage with respect to conventional ceramic overlay coatings. On the other hand, the process of thermal oxidation is a low cost and simple process to perform without changing the core metal or the shape of the implants. In the field of biomaterials, thermal oxidation has already been successfully performed for the development of zirconia forming alloys [8–15].

In this frame, a FeCrAl-based commercial available oxide dispersion strengthened (ODS) alumina forming alloy has been chosen as a candidate material for surgical implant devices, in particular for load-bearing joint replacements [16–18]. It is worth noting the absence of Ni, an allergenic element, in the bulk. Moreover, depending on the thermomechanical procedures, the Young's modulus of MA 956 may vary between 150 GPa, for the $\langle 1\,0\,0 \rangle$ texture, and 290 GPa, for the $\langle 1\,1\,1 \rangle$ texture. Since a Young's modulus closer to that of the bone is one of the material properties to consider seriously, the $\langle 1\,0\,0 \rangle$ texture was chosen as the microstructure under investigation.

MA 956 was especially suited for high temperature applications due to their excellent corrosive properties in aggressive environments, the latter being due to the ability to form a dense and adherent Al_2O_3 scale [29, and references therein]. The formation of a protective alumina scale on Fe-Cr-Al alloys, especially in the temperature range between 900 °C and 1100 °C, is complicated by transformations from the metastable γ- and θ-alumina phases to the most thermodynamically stable α-Al_2O_3 phase. This study has shown that thermal oxidation at 1100 °C gives rise to the formation of a nearly pure α-alumina scale on MA 956 since the earliest stage of oxidation. Probably the rate of these transformations at 1100 °C was so high that with the present

TABLE II Overview mechanical properties of conventional and candidate alloys for orthopaedic applications [25]

Alloy designation	Young's modulus (GPa)	Yield strength (MPa)	Ultimate strength (MPa)
Ti	105	692	785
Ti-6Al-4V	110	850–900	960–970
Ti-6Al-7Nb	105	921	1024
Ti-12Mo-6Zr-2Fe	74–85	1000–1060	1060–1100
Ti-13Nb-13Zr	79	900	1030
Ti-35Nb-5Ta-7Zr	55	530	590
Co-Cr-Mo	200–230	275–1585	600–1795
S.S. 316L	200	170–750	465–950
Bone	10–40	—	90–400

exposure times no other phases were present anymore or that these phases were only present as-nanocrystalline (amorphous) compounds. The scale growth kinetics obeyed a parabolic type law indicative of an oxide growth that is dominated by diffusion of reactants through a growing compact, dense and adherent scale. Only a compact oxide scale can protect the underlying substrate against aggressive environments. Structure and compositional analysis of the scale performed by the different techniques showed that on the top of the scale there has been formed nodules rich in Fe and Cr or Ti and Y. Ti and Y enrichment is more evident on the outer part and increases with treatment time, whereas Fe and Cr seem to appear just below the outer surface (Figs 3 and 6). These results agree well with other surface analyses performed showing significant amounts of titanium with some yttrium at the outer surface, in particular after longer exposure times. For shorter exposure times low quantities of iron and chromium were detected [23, 24, 30, 31].

The presence of defects might affect detrimentally the protective properties of the scale. The detailed cross-sectional analysis showed a dense and adherent oxide scale after 100 h exposure (Fig. 4). This observation is consistent with the very low porosity ($< 0.01\%$) expected for a 5 μm thick oxide scale [32]. Thicker oxide scales would progressively contain higher levels of porosity including poorer fracture toughness, which impair the good protective behavior. The presence of defects and/or conductive compounds in the oxide scale can also be analyzed by means of electrochemical techniques measuring the corrosion resistance of the material under investigation. In this study, the corrosion behavior of the material including the oxide layer has been investigated by the a.c. impedance method. This method offers a convenient way to evaluate the electrical properties of different metal/coatings systems [33–36]. The presence of defects in the scale like pores, voids, and cracks will detrimentally influence the protective capacity of the oxide layer. In that case, the absence of a dense and continuous alumina layer induces adverse body reactions due to release of metal ions from the metallic substrate, which in turn depends on the corrosion rate of the alloy. Therefore, it is vitally important to form a dense and adherent oxide layer protecting the underlying material against bodily fluids. The *In vitro* corrosion experiments have revealed good corrosion behavior of the α-Al_2O_3 layer formed on MA 956. The fact that the phase angle ($\approx -90°$) (Fig. 8) was more or less constant over the full frequency range denotes the formation of a nearly defect-free alumina layer. Concerning the as-received specimens, results have also shown good corrosion behavior due to the fact that this material spontaneously develops a passive film

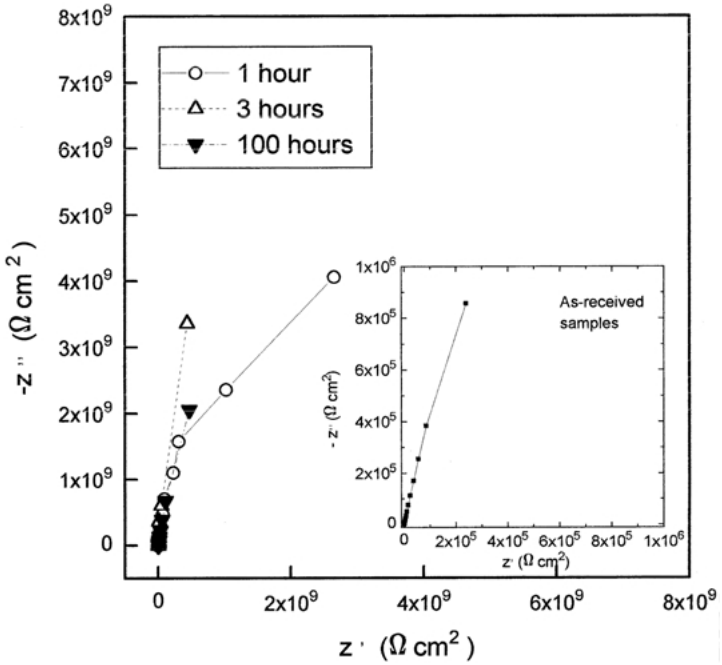

Figure 7 Nyquist diagram of as-received MA 956 and specimens oxidized for 1, 3 and 100 h after 4 days of immersion in the Hank's solution.

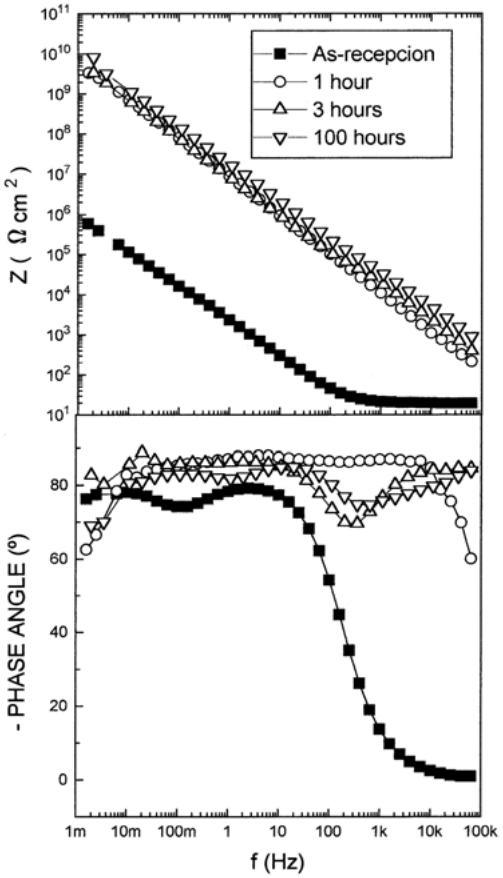

Figure 8 Bode diagram of as-received MA 956 and specimens oxidized for 1, 3 and 100 h after 4 days of immersion in the Hank's solution.

on the surface. Nevertheless, an α-Al_2O_3 layer is much more protective than the passive film formed in as-received condition. A more detail discussion concerning the interpretation of EIS data for this system can be found elsewhere [34, 37].

The surface and cross-sectional examinations and EIS have shown that no spallation of the alumina layer took place during cooling down the specimens from the oxidation temperature. This feature is significant considering that the alumina layer has to withstand very high compressive stresses resulting from both growth and thermal stresses incorporated during cooling. The magnitude of these stresses depends on a number of factors. For the given scale/alloy system and the set of experimental parameters used in this study it has been found that the residual stresses increase with increasing scale thickness [38]. For a scale formed upon 100 h exposure at 1100 °C on similar alloys compressive stresses of about 4.5 GPa have been determined [38, 39]. From a practical point of view, compressive stresses in the oxide scale will be desired with respect to the tensile residual stresses reported for conventional coatings [40]. Under service conditions, i.e. cyclic loading, implants are loaded mainly by bending stresses, in which both tension and compressive stresses are present. From data regarding tensile and compressive tests of preoxidized specimens, it was found that the alumina layer on this alloy is able to withstand, without cracking, tensile deformation [41] of about 1.4% and compressive deformation [42] of about 0.4%. The high compressive residual stress is expected also to increase the magnitude of the fatigue strength [18], since the oxide scale prevents plastic deformation of the substrate near the interface, thus retarding crack initiation. The presence of residual compressive stresses would be also advantageous when considering the wear behavior [43]. In this respect, small grain sizes of the alumina scale would be beneficial too [44].

In addition, the presence of an ceramic outer layer is very attractive because of alumina, specially the alpha structure, combines superior biocompatibility with high wear resistance, more than has been generally observed when metallic materials are used. Furthermore, due to the low thickness of the oxide layer, the product dimensions are not affected. However, it has been observed that the surface roughness increased with oxidation time, possibly due to the formation of nodules. The typical surface finish of implant bearing surfaces lies between 0.02 and 0.05 μm R_a, which is significantly lower than the surface roughness after thermal oxidation performed in this study (0.50 – 0.65 μm R_a). These nodules might also adversely influence the good wear behavior. This and possible ways of improvement are subject of further research.

5. Conclusions

Thermal oxidation treatment is a low cost process and simply to perform without changing the core metal or the shape of the implants. Results have shown that thermal oxidation of MA 956 for 1, 3 and 100 h at 1100 °C leads to the formation of an outer dense, non-porous and adherent α-Al_2O_3 scale, irrespective the exposure time. The oxidation process also induces to the formation of nodules on the top of the surface, rich in Y and Ti. Electrochemical corrosion experiments *in vitro* showed excellent protective properties of the formed oxide scale.

Acknowledgments

The authors wish to acknowledge the assistance of the staff of the Joint Research center, Institute for Health and Consumer Protection, in particular Dr P. N. Gibson (XRD), and Dr D. Gilliland (GDOES). Financial support from Spanish projects MAT95-0249-01 and MAT98-0944-01 is acknowledged.

References

1. S. SANTAVIRTA, D. NORDSTÖN, K. METSÄRINE and Y. KONTTINEN, *Clin. Orthop. Relat. Res.* **297** (1993) 100.
2. E. H. LEE, G. R. RAO, M. B. LEWIS and L. K. MANSUR, *Nucl. Instr. Meth. Phys. Res.* **74** (1993) 326.
3. G. L. SCHWARTZ, in Proc. 38th Annual Meeting Ortho. Research Soc., New Orleans, LA, February 5–8, 1990.
4. O. ZYWITZKI, G. HOETZSCH, F. FIETZKE and K. GOEDICKE, *Surf. Coat. Technol.* **82** (1996) 169.
5. K. HAYASHI, N. MATSUGUCHI, K. UENOYOMA, T. KANEMARU and Y. SUGIOKA, *J. Biomed. Mater. Res.* **23** (1989) 1247.
6. P. FRAISSINET, F. TOURENNE, N. ROUQUET, G. BONEL and P. CONTE, *J. Mater. Sci. Mater. Med.* **5** (1994) 491.
7. J. SKOGSMO, M. HALVARSSON and S. VUORINNEN, *Surf. Coat. Technol.* **54/55** (1992) 186.
8. J. A. DAVIDSON, A. K. MISHRA, P. KOVACS and R. A. POGGIE, *Bio-Medi. Mater. Engi.* **4** (1994) 231.
9. A. K. MISHRA and J. A. DAVIDSON, Advances in Biomaterials, **10** (1992) 111.

10. J. A. DAVIDSON and A. K. MISHRA in ''Surface Modification Technologies V'', edited by T. S. Sudarshan and J. F. Braza, (The Institute of Materials, 1992) p. 1.
11. J. A. DAVIDSON, in ''Ceramics in substitutive and reconstructive surgery'', edited by P. Vincenzini, Elsevier, Amsterdam (1991) p. 157.
12. J. A. DAVIDSON, U.S. Patent No. 5037438, August 1991.
13. J. A. DAVIDSON, and A. K. MISHRA, in Proc. Combined Meeting of the USA, Japan and Canada Orthopaedic Research Soc., Banff, Alberta, Canada, 1991.
14. A. K. MISHRA and J. A. DAVIDSON, in Proc. 9th Euro. Conf. On Biomaterials, Chester, UK, 1991.
15. V. BENEZRA, S. P. MANGIN, M. TRESKA, M. SPECTOR and L. W. HOBBS, in 24th Annual Meeting of the Society for Biomaterials, San Diego, California, USA, 1998.
16. M. L. ESCUDERO and J. L. GONZÁLEZ-CARRASCO, *Biomaterials* **15** (1994) 1175.
17. M. L. ESCUDERO, M. F. LÓPEZ, J. RUIZ, M. C. GARCÍA-ALONSO and H. CANAHUA, *J. Biomed. Mater. Res.* **31** (1996) 313.
18. J. L. GONZÁLEZ-CARRASCO, M. L. ESCUDERO, J. CHAO and M. C. GARCÍA-ALONSO, *Mater. Manu. Proc.* **13** (1998) 431.
19. H. OONISHI, H. OKABE, T. IKE and E. TSUJI, *Ann NY Acad. Sci.* **523** (1988) 38.
20. J. CHAO, M. C. CRISTINA, J. L. GONZÁLEZ-CARRASCO and G. GONZÁLEZ-DONCEL, *Rev. Metal. Madrid* **34** (1998) 211.
21. J. CHAO, and G. GONZÁLEZ-DONCEL, *Rev. Metal. Madrid* **34** (1998) 216.
22. J. CHAO, M. C. CRISTINA, J. L. GONZÁLEZ-CARRASCO and G. GONZÁLEZ-DONCEL, in *Materials for Advanced Power Engineering 1998*, edited by J. Lecomte-Beckers, F. Shubert and P. J. Ennis, Forschungszentrum Jülich GmbH, Central Library, *Proc. 6th Liège Conference*, Vol. 5 Part II, pp. 827–834.
23. M. C. GARCÍA-ALONSO, PhD-Thesis, Universidad Autónoma de Madrid, Spain, 1997.
24. M. C. GARCÍA-ALONSO, J. L. GONZÁLEZ-CARRASCO, M. L. ESCUDERO and J. CHAO, *Oxid. Met.* **53** (2000) 77.
25. M. LONG, and H. J. RACK, *Biomaterials* **19** (1998) 1621.
26. J. A. DAVIDSON, *Clin. Orthop. Relat. Res.* **294** (1993) 361.
27. J. E. LEMONS, *Surf. Coat. Technol.* **103–104** (1998) 135.
28. J. RIEU, *Clin. Mater.* **12** (1993) 227.
29. W. J. QUADAKKERS, Journal de Physique IV, Colloque C9, supplement au Journal de Physique III, **3** (1993) 177.
30. M. F. LÓPEZ, A. GUTIERREZ, M. C. GARCÍA-ALONSO and M. L. ESCUDERO, *J. Mater. Res.* **13** (1998) 3411.
31. W. J. QUADAKKERS, A. ELSCHNER, H. HOLZBRECHER, K. SCHMIDT, W. SPEIER and H. NICKEL, *Mikrochim. Acta* **107** (1992) 197.
32. J. P. WILBER, J. R. NICHOLLS and M. J. BENNETT, in ''Microscopy of Oxidation 3'', edited by S. B. Newcomb and J. A. Little (The Institute of Materials, London, 1996) p. 207.
33. J. PAN, C. LEYGRAF, R. F. A. JARGELIUS-PETTERSSON and J. LINDEN, *Oxid. Met.* **50** (1998) 431.
34. M. L. ESCUDERO, J. L. GONZÁLEZ-CARRASCO, M. C. GARCÍA-ALONSO and E. RAMÍREZ, *Biomaterials* **16** (1995) 735.
35. K. J. BUNDY, J. DILLARD and R. LUEDEMANN, *Biomaterials* **14** (1993) 529.
36. I. THOMPSON, and D. CAMPBELL, *Corr. Sci.* **36** (1994) 187.
37. M. C. GARCÍA-ALONSO, M. L. ESCUDERO, J. L. GONZÁLEZ-CARRASCO and J. CHAO, *Biomaterials* **21** (2000) 79.
38. R. J. CHRISTENSEN, V. K. TOLPYGO and H. J. GRABKE, *Acta Mater.* **45** (1997) 1761.
39. J. P. BANKS, D. D. GOHIL, H. E. EVANS, D. J. HOLL and S. R. J. SAUNDERS, in ''Materials for Advanced Power Engineering'', D. Coutsouradis *et al*., Part II, (Kluwer Academic Press, The Netherlands, 1999) p. 1543.
40. J. BRENE, Y. ZHOU and L. GROH, *Biomaterials* **16** (1995) 239.
41. J. CHAO, J. L. GONZÁLEZ-CARRASCO, J. IBAÑEZ, M. L. ESCUDERO and G. GONZÁLEZ-DONCEL, *Metall. Mater. Trans.* **27A** (1996) 3809.
42. J. CHAO and J. IBAÑEZ (unpublished results).
43. S. J. BULL, R. KINGSWELL and K. T. SCOTT, *Surf. Coat. Technol.* **82** (1996) 218. J. C. SCHNEIDER, in ''High Tech Ceramics'', de. P. Vincenzini (Elsevier Science Publishers B.V., Amsterdam, 1987) p. 2581.

Received 25 October 1999
and accepted 27 June 2000